Journal of Controlled Release 200 (2015) 188–200

Contents lists available at ScienceDirect

Journal of Controlled Release

journal homepage: www.elsevier.com/locate/jconrel

Tumor-penetrating peptide fused EGFR single-domain antibody enhances cancer drug penetration into 3D multicellular spheroids and facilitates effective gastric cancer therapy

Huizi Sha [a], Zhengyun Zou [a], Kai Xin [a], Xinyu Bian [a], Xueting Cai [b,c], Wuguang Lu [b,c], Jiao Chen [b,c], Gang Chen [d], Leaf Huang [e], Andrew M. Blair [e], Peng Cao [b,c,**], Baorui Liu [a,*]

[a] The Comprehensive Cancer Center of Drum-Tower Hospital, Medical School of Nanjing University & Clinical Cancer Institute of Nanjing University, Nanjing, China
[b] Laboratory of Cellular and Molecular Biology, Jiangsu Province Academy of Chinese Medicine, Nanjing, China
[c] Jiangsu Province Hospital on Integration of Chinese and Western Medicine, Nanjing University of Chinese Medicine, Nanjing, China
[d] State Key Laboratory of Natural Medicines, School of Life Science and Technology, China Pharmaceutical University, Nanjing, China
[e] Division of Molecular Pharmaceutics and Center for Nanotechnology in Drug Delivery, Eshelman School of Pharmacy, University of North Carolina at Chapel Hill, Chapel Hill, USA

ARTICLE INFO

Article history:
Received 11 October 2014
Received in revised form 2 December 2014
Accepted 25 December 2014
Available online 30 December 2014

Chemical compounds studied in this article:
Paclitaxel (PubChem CID: 36314)
Doxorubicin hydrochloride (PubChem CID: 443939)
Fluorescein isothiocyanate (PubChem CID: 18730)
Isopropyl β-D-1-thiogalactopyranoside (PubChem CID: 656894)

Keywords:
Recombinant protein
iRGD
Anti-EGFR sdAb
Multicellular spheroids
Drug penetration
Drug delivery

ABSTRACT

Human tumors, including gastric cancer, frequently express high levels of epidermal growth factor receptors (EGFRs), which are associated with a poor prognosis. Targeted delivery of anticancer drugs to cancerous tissues shows potential in sparing unaffected tissues. However, it has been a major challenge for drug penetration in solid tumor tissues due to the complicated tumor microenvironment. We have constructed a recombinant protein named anti-EGFR-iRGD consisting of an anti-EGFR VHH (the variable domain from the heavy chain of the antibody) fused to iRGD, a tumor-specific binding peptide with high permeability. Anti-EGFR-iRGD, which targets EGFR and αvβ3, spreads extensively throughout both the multicellular spheroids and the tumor mass. The recombinant protein anti-EGFR-iRGD also exhibited antitumor activity in tumor cell lines, multicellular spheroids, and mice. Moreover, anti-EGFR-iRGD could improve anticancer drugs, such as doxorubicin (DOX), bevacizumab, nanoparticle permeability and efficacy in multicellular spheroids. This study draws attention to the importance of iRGD peptide in the therapeutic approach of anti-EGFR-iRGD. As a consequence, anti-EGFR-iRGD could be a drug candidate for cancer treatment and a useful adjunct of other anticancer drugs.

1. Introduction

Gastric cancer is one of the world's leading causes of cancer-related death with a high incidence and mortality rate, particularly in Eastern Asia [1,2]. Despite recent advances in cancer therapy, such as chemotherapy, radiotherapy and biological immune therapy, most advanced malignancies still remain incurable. Thus, the research and development of new therapeutics is essential.

With the advent of molecular engineering and phage display technology, more antibodies have been explored. Antibodies have different formats and VHH as a minimal functional format has some advantages, such as: lower immunogenicity, facile genetic manipulation, high physicochemical stability, recognition of hidden antigenic sites and high expression levels. Therefore, there seems to be a trend in therapeutic and diagnostic antibodies towards smaller antigen-binding antibody formats [3,4]. The variable domain from the heavy chain of the antibody (VHH), often called a single domain antibody (sdAb) [5] or nanobody [6] due to its size in the nanometer range, is considered to be the smallest naturally derived antigen-binding fragment [7]. Human tumors frequently express high levels of epidermal growth factor receptor (EGFR), which has been associated with a poor prognosis when overexpressed [8]. EGFR (ErbB1, HER1) is a 170-kDa transmembrane tyrosine kinase receptor, overexpressed in a wide variety of human

* Correspondence to: B. Liu, The Comprehensive Cancer Center of Drum-Tower Hospital, Medical School of Nanjing University & Clinical Cancer Institute of Nanjing University, Zhongshan Road 321, Nanjing 210008, China.
** Correspondence to: P. Cao, Laboratory of Cellular and Molecular Biology, Jiangsu Province Academy of Traditional Chinese Medicine, 100#, Shizi Street, Hongshan Road, Nanjing 210028, China.
E-mail addresses: baoruiliu@nju.edu.cn (B. Liu), pcao79@yahoo.com (P. Cao).

http://dx.doi.org/10.1016/j.jconrel.2014.12.039
0168-3659/

cancers including 27.4% of 511 gastric cancer tissues [9]. Progress in genetic engineering has guided the way for development of various EGFR inhibitors including monoclonal antibodies, (cetuximab, panitumumab, etc.), tyrosine-kinase inhibitors (gefitinib, erlotinib, lapatinib, etc.), antisense oligonucleotides and sdAbs [10].

Although targeted delivery of anticancer drugs to cancerous tissues shows potential in sparing unaffected tissues, it is still a major challenge for the targeted therapeutic to penetrate deep into solid tumor tissues. In solid cancers, the homeostatic regulation of tissues breaks down, cancer cells are in the state of hypoxia, interstitial fluid pressure increases [11–14], and the extracellular matrix (ECM) hinders the movement of drugs and molecules into the tumor tissue [15–17].

It has been reported that the tumor-penetrating and cell-internalizing peptide iRGD (sequence: CRGDKGPDC) contains both a RGD (Arg-Gly-Asp) domain and a CendR motif (R/KXXR/K). It first binds to αvβ3 and αvβ5 integrins, which are expressed highly in tumor vessels and many different types of cells in the tumor [18]. Subsequently, iRGD is proteolytically cleaved to CRGDK/R. The truncated peptide loses affinity for the primary receptor integrin, and binds to neuropilin-1 (NRP-1), triggering a cell internalization and tissue penetration pathway [19,20].

Since Sutherland et al. [21,22] established multicellular spheroids (MCS) in the 1970s, this three-dimensional (3D) MCS in vitro tumor model has been demonstrated as a practical and simple model that reflects many of the properties of natural solid tumors. The 3D culture conditions in MCS can produce an ECM [23,24], which creates a major obstacle for drug penetration into tumor tissues. In addition, large MCS (>200 μm in diameter) have been demonstrated to form three different regions: proliferating periphery cell populations, a viable and quiescent intermediate zone, and a necrotic core from the outside in [25,26]. Furthermore, Minchinton et al. [27] mentioned that, MCS were an ideal platform for studying drug penetration, along with multilayered cell cultures and in vivo methods.

In this study, an anti-EGFR sdAb selected by phage display was used as a ligand to interact with EGFR. To efficiently deliver anti-EGFR sdAbs into the tumor and overcome the difficulty of poor penetration of anticancer drugs in solid tumors [27,28], we introduced a C-end Rule peptide iRGD to an anti-EGFR sdAb. Afterwards, the anticancer activity of the recombinant proteins anti-EGFR and anti-EGFR-iRGD were examined. Penetration of anti-EGFR and anti-EGFR-iRGD through both MCS culture system and in vivo methods was then evaluated. To study the effect of anti-EGFR-iRGD on drug delivery and efficacy, we also administered the protein as a combination therapy with several types of cancer drugs, such as DOX, bevacizumab, nanoparticles in a 3D multicellular spheroid model.

2. Materials and methods

2.1. Reagents, cell lines, and tumors

Doxorubicin hydrochloride (DOX) was purchased from Shenzhen Main Luck Pharmaceuticals Inc. (Shenzhen China). Paclitaxel liposome was obtained from Nanjing Si Ke Pharmaceutical Co., Ltd. (Nanjing, China), bevacizumab and cetuximab were purchased from Roche (Basel, Switzerland) and Merck (Darmstadt, Germany). siRNA targeting human EGFR mRNA (GenBank Accession No. NM_005228), integrin αv mRNA (GenBank Accession No. NM_001144999), and NRP-1 mRNA (GenBank Accession No. NM_001024628) were designed and synthesized by Guangzhou RiboBio Company (Guangzhou, China). Antibodies were purchased from Cell Signaling Technology (USA) (for human EGFR antibody), Signalway Antibody (USA) (for p-EGFR Tyr1172), Novus biologicals (USA) (for human αvβ3 antibody), and Abcam (USA) (for human NRP-1 antibody). Mouse monoclonal anti-human CD31 and rat monoclonal anti-mouse CD31 were purchased from Gene Tech Company Limited (Shanghai, China) and BD Pharmingen (San Jose, California). An Alexa 594 conjugated donkey anti-mouse secondary antibody and donkey anti-rat secondary antibody were purchased from Abcam (USA) and Molecular Probes (Eugene, Oregon). Full length DNA for anti-EGFR in the vector pSJF2 was a gift from Dr. Shenghua Li at Tianjin International Joint Academy of Biotechnology and Medicine (Tianjin, China). 3-(4,5-Dimethylthiazol-2-yl)-2,5-diphenyltetrazolium bromide (MTT) for the cell viability assay was obtained from Sigma-Aldrich (USA). Fluorescein isothiocyanate (FITC) and coumarin-6, were obtained from Sigma Chemical Co (USA). All other chemicals were used as received without further treatment.

Human gastric adenocarcinoma cell line BGC-823, human epithelial colorectal adenocarcinoma cell line Caco-2, human breast adenocarcinoma cell line MCF-7 and murine hepatic cancer cell line H22, were purchased from the Cell Bank of Shanghai Institute of Biochemistry and Cell Biology. BGC-823 and H22 were cultured in RPMI 1640 medium supplemented with 10% fetal calf serum, while other cells were cultured in DMEM-medium (for MCF-7 cells) or MEM-medium (for Caco-2 cells), supplemented with 10% fetal bovine serum, 100 U/mL penicillin and 100 μg/mL streptomycin, and incubated at 37 °C and 5% CO_2 (all available from Invitrogen, Grand Island, NY, USA). All animal procedures were carried out in compliance with guidelines set by the Animal Care Committee at Drum Tower Hospital (Nanjing, China). Five million BGC-823 gastric cancer cells in 0.1 mL PBS were subcutaneously injected in the lower right axilla of athymic nude BALB/c mice (5–6 weeks, male, 18–22 g), while 5 million H22 cells were subcutaneously injected in the right axilla of ICR mice (4–5 weeks, male, 18–22 g) to produce xenograft tumors. Tumor volumes were calculated from 2 diameter measurements using a digital vernier caliper and the formula: tumor volume = (length × width^2) / 2, where length is the longest dimension and width is the widest dimension.

2.2. Preparation and characterization of recombinant proteins anti-EGFR and anti-EGFR-iRGD

Recombinant proteins anti-EGFR and anti-EGFR-iRGD were prepared as follows. The anti-EGFR sequence was cloned into the bacterial expression vector pET28a with a hexahistidine (His) tag placed at the N-terminus of anti-EGFR. To enhance cell- and tissue-penetration of anti-EGFR, oligonucleotides encoding iRGD were synthesized and ligated downstream of oligonucleotides encoding the anti-EGFR, with a glycine–serine linker (Asp) 4 Lys, i.e., G4S tag, placed in between. Both of the recombinant plasmids were confirmed by DNA sequencing. Proteins were expressed in *Escherichia coli* (*E. coli*) BL21 (DE3) after induction by isopropyl β-D-1-thiogalactopyranoside. The cells were then harvested by centrifugation, and suspended and disrupted by sonication. The supernatant of the cell lysate was further purified using nickel–nitrilotriacetic acid affinity chromatography under native conditions by the ÄKTA fast protein liquid chromatography system according to the manufacturer's instructions. The eluted fractions were analyzed by 4% to 15% sodium dodecyl sulfate-polyacrylamide gel electrophoresis (SDS-PAGE) and confirmed by XIMA MALDI-TOF (Shimadzu Kratos, Manchester, UK). Labeled recombinant proteins were prepared by conjugating with FITC at the amine groups of lysine. The labeled protein was dialyzed and filtered (0.22 μm).

2.3. Initial model building and molecular dynamics

To exhibit recombinant proteins intuitively, 3D structures of anti-EGFR and anti-EGFR-iRGD were modeled using the Accelrys Discovery Studio 4.0, based on the template of B39 VHH (PDB: 4NC2_B) [29]. Molecular dynamics simulations were conducted to refine the modeled 3D structures with AMBER 12.0. Energy minimization was performed in order to remove possible poor contacts between the solute and solvent (5000 steps for the water molecules followed by 5000 steps for the whole system). Molecular dynamics simulations were then conducted at constant temperature (300 K) and pressure (1.0 atm) with a time

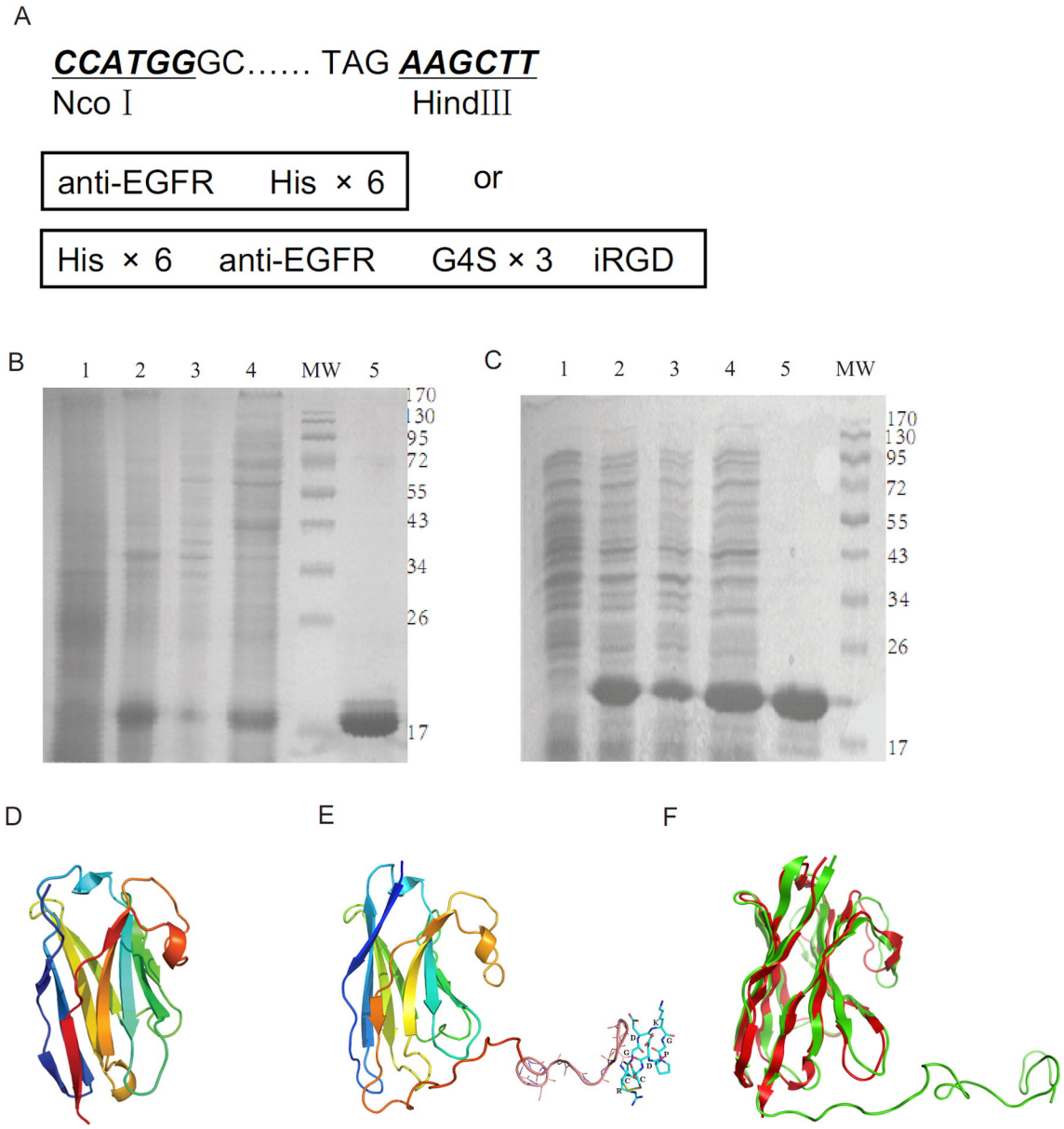

Fig. 1. Expression and purification analysis of recombinant proteins anti-EGFR and anti-EGFR-iRGD. A, restriction sites are indicated underlined, the His × 6 tag and G4S tag are shown in the boxes. B and C, anti-EGFR and anti-EGFR-iRGD purified from BL21 (DE3) lysate. Lane 1: bacterium without IPTG introduction; Lane 2: bacterium introduced with 1 mM IPTG at 37 °C; Lane 3: the precipitation of the ultrasonic lysate; Lane 4: the supernatant of the ultrasonic lysate; Lane 5: purified anti-EGFR (B) or anti-EGFR-iRGD (C) with nickel-affinity chromatography. D and E, the structures of the recombinant proteins anti-EGFR (D) and anti-EGFR-iRGD (E) after homology modeling and molecular dynamics simulations. F, superimposition of anti-EGFR and anti-EGFR-iRGD.

step of 2 fs. After 1 ns equilibration, production simulations for all systems were conducted for 10 ns. Other parameters can be referred to in our previous publication [30].

2.4. Antigen–antibody binding assay and competitive binding assay

To investigate the binding profiles of recombinant proteins anti-EGFR and anti-EGFR-iRGD with human EGFR, surface plasmon resonance analysis was conducted as previously described [31]. BGC-823 cells in the logarithmic phase were seeded at a density of 50% confluence per well into 24-well chamber slides. Cells were transfected with 50 nmol/L siRNAs directed against EGFR, αvβ3 and NRP-1, respectively. Forty-eight hours later, cells were blocked in phosphate-buffered saline (PBS) supplemented with 5% bovine serum albumin and then incubated at 37 °C with FITC-labeled anti-EGFR-iRGD for 1 h. The cells were then washed three times with PBS (pH 7.4) and fixed before labeling the nuclei with Hoechst 33258. Next, the cells were observed with a laser scanning confocal microscope (LSCM) (Zeiss LSM 710). Simultaneously, BGC-823 cells of the same treatment group were harvested and analyzed using a FACScan laser flow cytometer (Guava easycyteHT, Millipore, CA). The competitive binding assay was done as follows: BGC-823 cells were transfected with siRNAs and blocked with 5% bovine serum albumin as described above. The cells were then incubated with a sub-saturated concentration of anti-EGFR-iRGD-FITC and the appropriate concentration of competing EGFR monoclonal antibody cetuximab or iRGD at 37 °C for 1 h. After fixing and nucleus staining, the cells were observed with a fluorescence microscope. Similarly, with the same treatment of competing cetuximab or iRGD, the alterations of the mean channel fluorescence were analyzed by a FACScan laser flow cytometer.

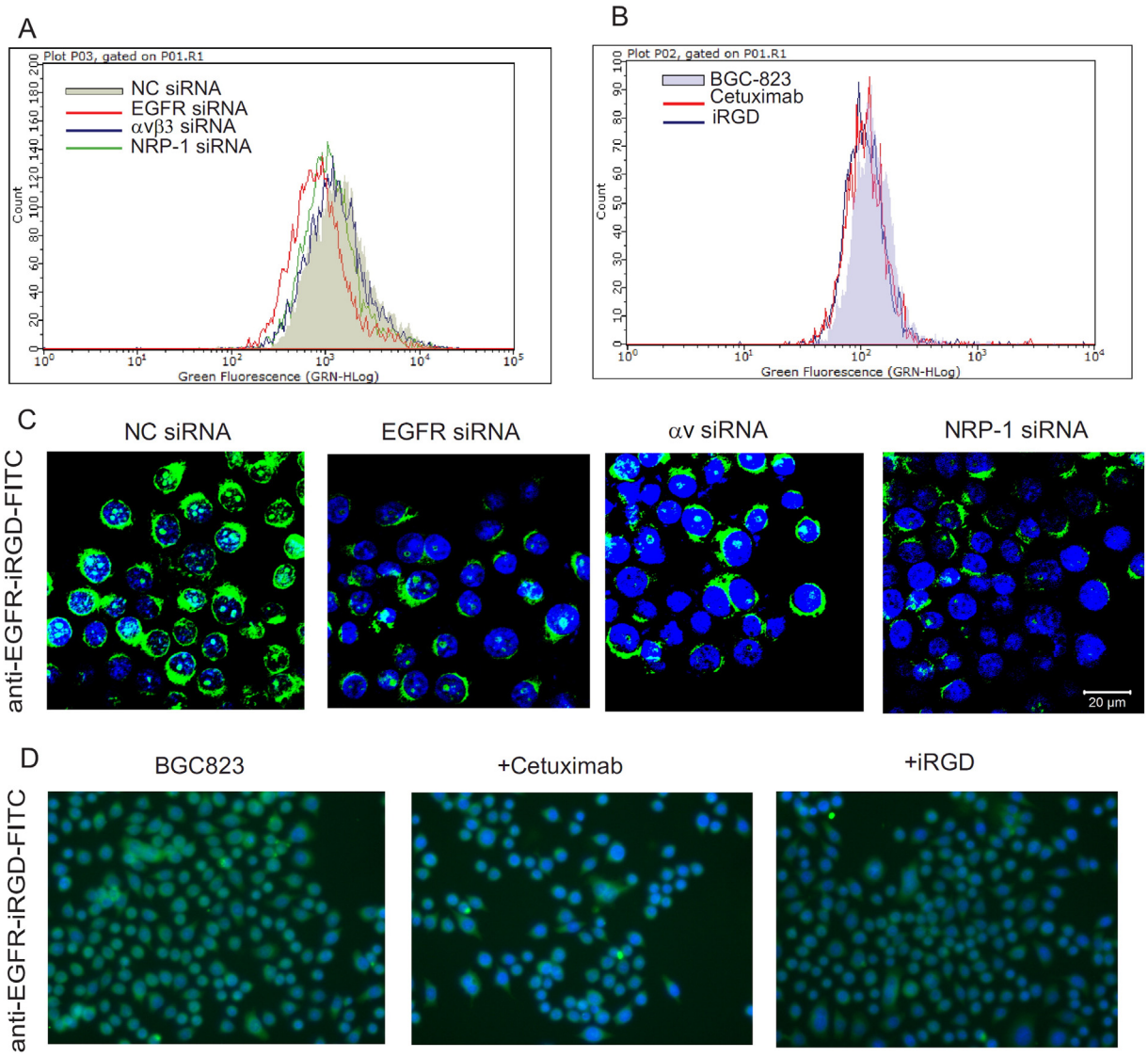

Fig. 2. Evaluating the antigen-binding profile of recombinant protein anti-EGFR-iRGD. A and C, after transfection with siRNA to silence the expression of EGFR, αvβ3 or NRP-1, the binding profile of BGC-823 cells with FITC labeled anti-EGFR-iRGD was analyzed by flow cytometry analysis (A) and LSCM (C). B and D, the analyses of BGC-823 tumor cells by competitive binding assay are shown according to FITC labeled anti-EGFR-iRGD. BGC-823 cells were incubated with a sub-saturating concentration of anti-EGFR-iRGD-FITC and an indicated concentration of competing mAb cetuximab or iRGD. The fluorescence images (D) are shown and the alterations of the mean channel fluorescence on the surface of BGC-823 cells were detected by flow cytometry analysis (B). Scale bar in C = 20 μm and D (×400).

2.5. Formation of BGC823 MCS and growth inhibition study in MCS

In order to produce MCS, matrigel (BD Bioscience, USA) was used as previously described [32]. A layer of matrigel (300 μL/well) was coated on the bottom of a 24-well plate at 4 °C and later put in a 37 °C atmosphere for 30 min to assure that the matrigel had solidified. BGC-823 monolayer cells incubated as mentioned above were trypsinized and harvested to give a single-cell suspension. In this case, 5×10^5 cells in 1 mL of RPMI 1640 medium were placed in a well of the pre-treated 24-well plate. Cells were incubated at 37 °C in a 5% CO_2 humidified atmosphere and the culture medium was replaced every day. BGC-823 MCS (approximately 200 μm in diameter) formed spontaneously in 7 days.

Tumor MCS with 3D architecture are often used to predict the drug antitumor effect as an ideal platform mimicking solid tumors [33]. Comparing the cytotoxicities of recombinant proteins and indicated cancer drugs (DOX, bevacizumab, paclitaxel liposome) was done in MCS using a growth inhibition assay [34]. The MCS of about 200 μm in diameter were incubated with different treatments, as indicated, at 37 °C for 7 days. As an indication of MCS proliferation, the diameters of spheroids were measured every day after images were taken using an optical microscope.

2.6. Penetration in MCS and in tumor tissue

The distributions of anti-EGFR and anti-EGFR-iRGD in MCS were determined by LSCM. For each experiment, around 20 BGC-823 spheroids (about 200 μm in diameter) were collected and transferred to a 5 mL Eppendorf tube. MSC were incubated with FITC-labeled anti-EGFR and anti-EGFR-iRGD for 6 h or 24 h at 37 °C. Proper concentrations of proteins, DOX and DOX combination with indicated proteins were added respectively, to the suspension of spheroids, and co-cultured for the indicated time. Coumarin-6 loaded poly(ethyleneglycol)-poly(ε-caprolactone) nanoparticles (PEG-PCL-Coumarin-6-NP) were prepared as previously described [35]. Similarly, proper concentrations of proteins, PEG-PCL-Coumarin-6-NP and PEG-PCL-Coumarin-6-NP combination with indicated proteins were added respectively. The semi-

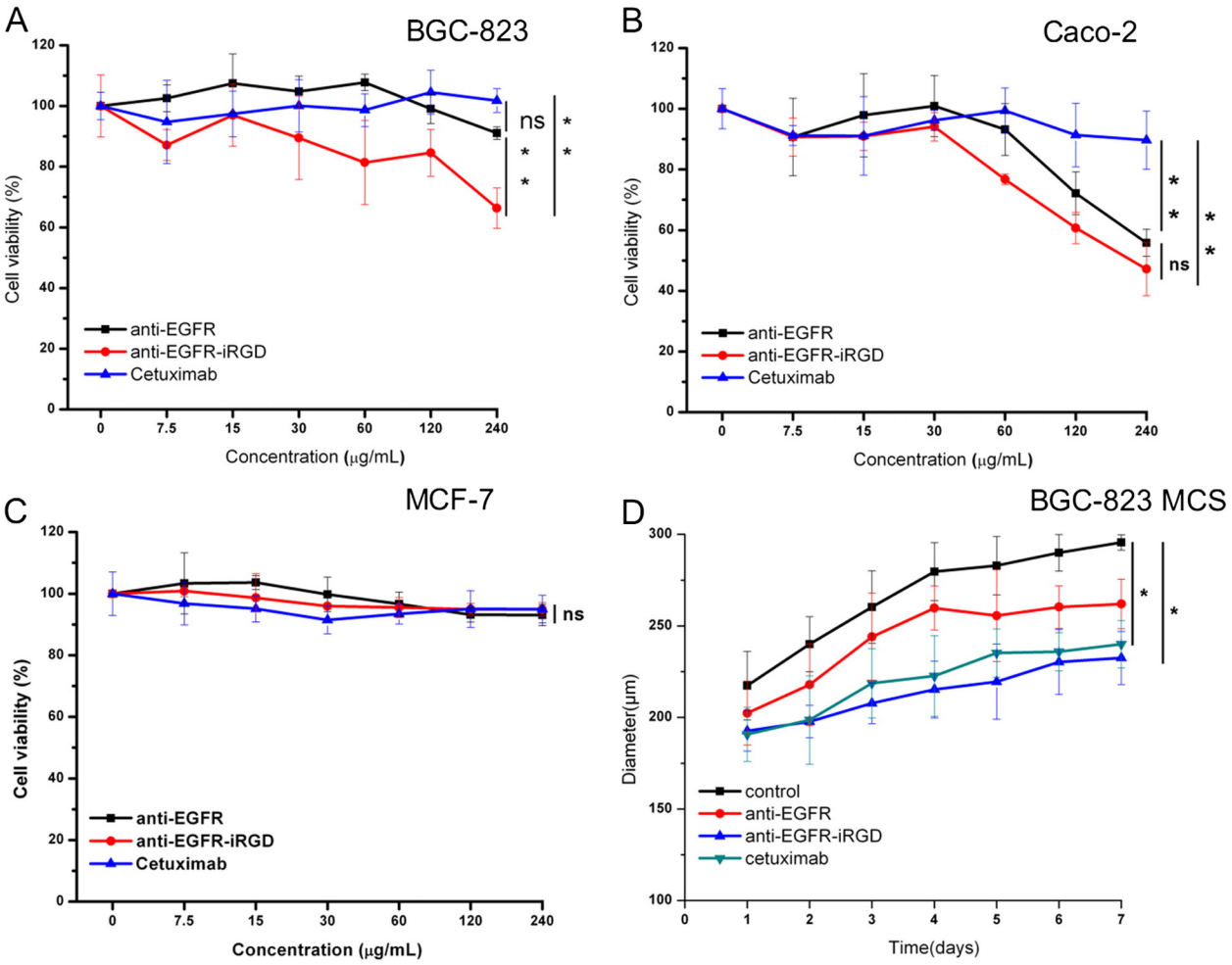

Fig. 3. Cytotoxicity of protein anti-EGFR or anti-EGFR-iRGD in tumor cell lines and MCS. A, B and C, anti-EGFR, anti-EGFR-iRGD, or cetuximab of various concentrations were added to the BGC-823 (A), Caco-2 (B) or MCF-7 (C) cell suspensions and incubated for 48 h. Cell viability was measured by MTT assay. D, growth inhibition assay in BGC-823 MCS. Growth curves of MCS after various indicated treatment. All data were expressed as the mean ± standard deviation (SD), n = 4. Data represent the means of three independent experiments. Statistical analyses were performed using the Student *t* test and one-way ANOVA. *, $p < 0.05$, **, $p < 0.01$, ns, not significant.

quantitative analysis of mean fluorescence intensity of MCS was made using the ZEN 2008 program.

Due to overexpression of EGFR, NRP-1 and integrin in BGC-823 cells (Supplementary Fig. S3A, B, and C), H22 bearing ICR mice were used as models to evaluate iRGD effects [34,36]. We made use of two animal models to trace the location of proteins and investigate the penetration of recombinant proteins. BALB/c mice and ICR mice were subcutaneously inoculated with either BGC-823 cells or H22 cells, when tumors reached about 400 mm^3, the FITC-labeled anti-EGFR and anti-EGFR-iRGD were injected into BGC-823 tumor-bearing mice and H22 tumor-bearing mice via a tail vein, respectively. Mice were sacrificed and tumors were harvested 1 h after administration. Immunofluorescence for frozen tumor tissue sections was conducted as previously described [34,36,37]. The sections were observed with LSCM.

2.7. In vivo antitumor effect and safety of anti-EGFR and anti-EGFR-iRGD

BALB/c mice were subcutaneously injected with BGC-823 gastric cancer cells as mentioned above. The mice with tumors of about 100 mm^3 were randomly divided into 4 groups with each group containing 8 mice (no statistically significant difference in tumor volume among groups). The day of randomization was designated as "Day 0". Proteins were diluted in PBS at 1.2 mg/mL, and the mice were treated by intraperitoneal injection every 3 days with recombinant protein anti-EGFR, anti-EGFR-iRGD or cetuximab at 12 mg/kg on the first day of treatment (day 0) and either 6 mg/kg or PBS each subsequent injection. The injections were given every 3 days (a total of 4 injections in the BGC-823 model). All of the mice were observed daily and the body weight and tumor volume (by a digital vernier caliper) were measured every 3 days. Mice were sacrificed at the end of the experiment. Both tumor tissues and main organs (heart, liver, spleen, lung and kidney) were dissected for histology observation on the 12th day after treatment (n = 3 mice per group). After being fixed in 10% neutral buffered formalin, the tissues were embedded in paraffin, sectioned at a thickness of 5 μm, and stained by H&E (hematoxylin and eosin). The proliferating cell nuclear antigen (PCNA) immunohistochemistry was used to evaluate the proliferation of the cells in the tumors. The slices obtained were examined using optical microscopy.

3. Results

3.1. Construction, production and characterization of recombinant protein

Anti-EGFR and anti-EGFR-iRGD genes were separately cloned in frame between the NcoI and HindIII restriction sites of the pET28a plasmid, from which recombinant proteins containing His tag were produced (Fig. 1A). Most of the recombinant proteins were detected as soluble proteins (Fig. 1B and C), successfully induced in *E. coli* BL21

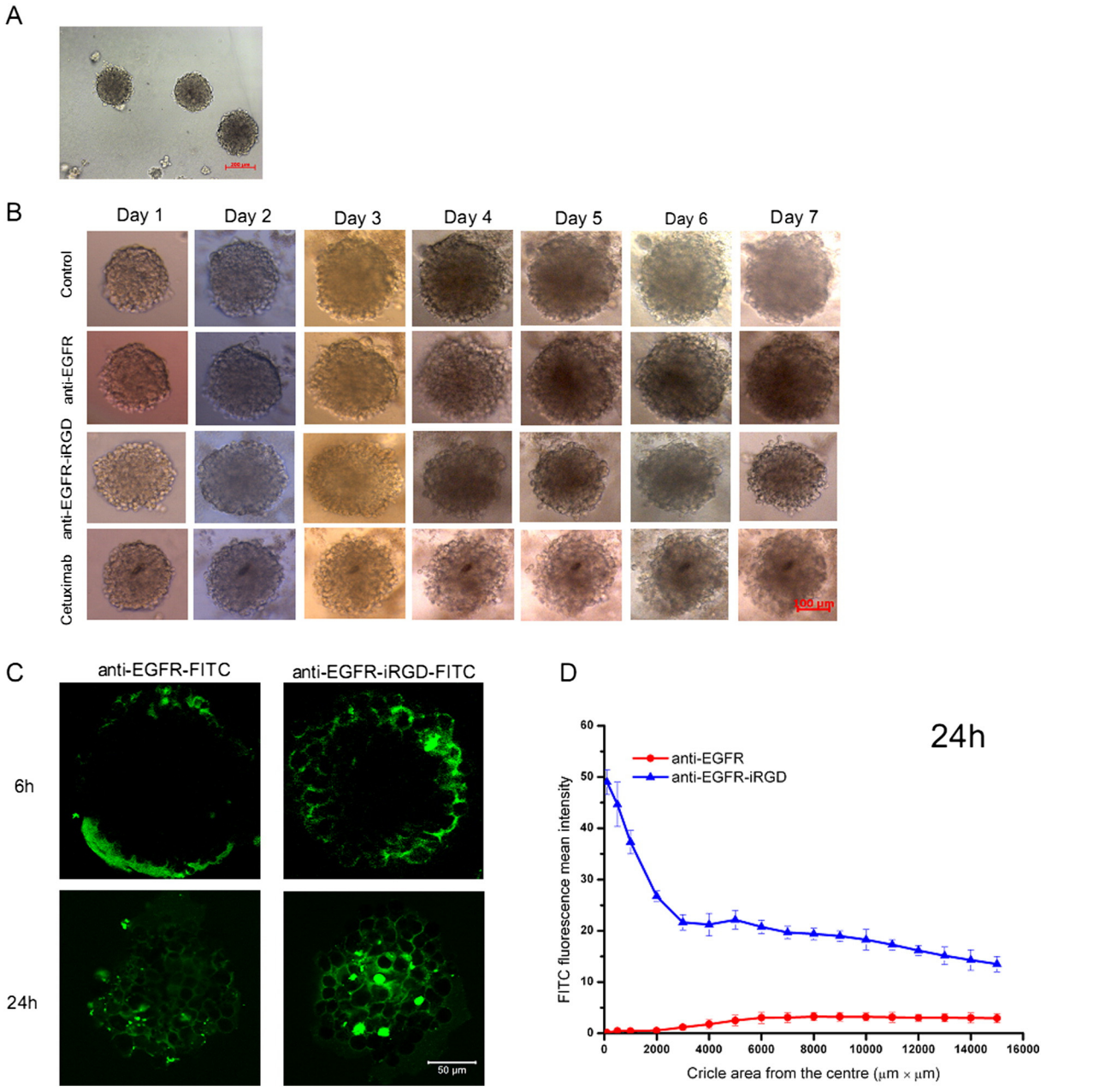

Fig. 4. The image of BGC-823 MCS and the penetration of proteins in BGC-823 MCS. A, the image of BGC-823 MCS captured by an optical microscope; scale bar = 200 μm. B, representative images of MCS treated with culture medium, anti-EGFR, anti-EGFR-iRGD or cetuximab. MCS were cultured in RPMI 1640 medium as a control; scale bar = 100 μm. C, LSCM images of BGC-823 MCS incubated with FITC-labeled anti-EGFR and FITC-labeled anti-EGFR-iRGD for 8 h and 24 h. D, the alterations of the mean fluorescence intensity from the center region to the periphery of the MCS cultured with anti-EGFR-FITC and anti-EGFR-iRGD-FITC after 24 h incubation. Data are represented as mean ± SD (n = 3). ***, $p < 0.001$. Scale bar in C, 50 μm.

(DE3) and purified respectively. Proteins migrated as major bands at 16 kDa (anti-EGFR) and 18 kDa (anti-EGFR-iRGD) in Coomassie blue-stained SDS-PAGE (Fig. 1B and C). The molecular weight of anti-EGFR and anti-EGFR-iRGD was detected as 16171 and 18050 by MALDI-TOF (data not shown), which is consistent with the values expected from the recombinant protein sequence. These results confirm the successful expression of soluble anti-EGFR and anti-EGFR-iRGD.

The sequence identity between anti-EGFR and B39 VHH was 76.8% (Supplementary Fig. S1), while linker G4S and iRGD had no template. The 3D structures were then constructed by homology modeling using B39 VHH as the template to determine whether iRGD could influence the structure of the sdAb. Molecular dynamics simulations were conducted to refine the models. Linker G4S and iRGD stationed at the outside of anti-EGFR, as a consequence did not intertwine with the sdAb (Fig. 1D and E). When superimposed, most regions of anti-EGFR overlapped very well with anti-EGFR of anti-EGFR-iRGD (Fig. 1F), and showed no obvious difference from the overall structure of the sdAb. The root mean square deviation of Cα is 1.757 Å, which implies that the iRGD motif does not affect the 3D structure of the sdAb.

3.2. Evaluating the antigen-binding profiles of recombinant proteins

The binding profiles of recombinant protein anti-EGFR and anti-EGFR-iRGD were analyzed using the SPR-based biosensor by flowing them separately over the same surface of human EGFR-extracellular domain (Supplementary Fig. S2). The k_D of anti-EGFR and anti-EGFR-iRGD was in the same order of magnitude (Supplementary Table S1), which means the modification of anti-EGFR would not affect its biological activity, i.e., the iRGD domain would not weaken the affinities to EGFR of anti-EGFR-iRGD.

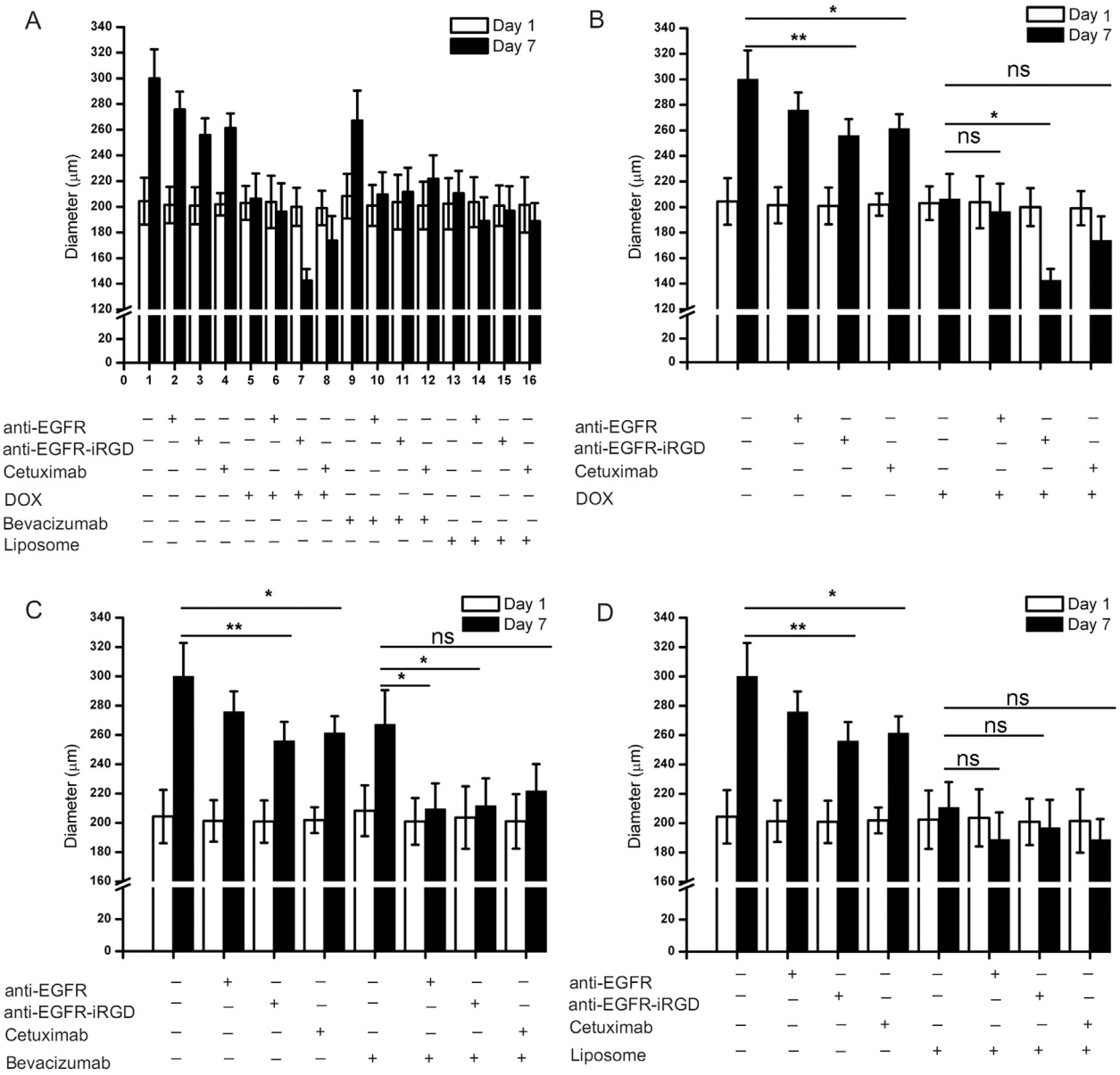

Fig. 5. Growth inhibition assay in BGC-823 MCS. Growth curves of MCS after various indicated treatment. B, C and D are part of A. All data were expressed as the mean ± standard deviation (SD), n = 4. Data represent the means of three independent experiments. Statistical analyses were performed using the Student *t* test and one-way ANOVA. *, $p < 0.05$, **, $p < 0.01$, ns, not significant.

The indicated treatments for the best silencing effects (50 nM of EGFR siRNA-No. 1, 50 nM of αvβ3 siRNA-No. 1, and 50 nM of NRP-1 siRNA-No. 2) were conducted following the manufacturer's description of Lipofectamine® 2000. The silencing effects were confirmed by Western blotting (Supplementary Fig. S3A, B and C). It was found that BGC-823 cells co-incubated with the EGFR, αvβ3, and NRP-1 siRNA took up less anti-EGFR-iRGD-FITC than the negative control (NC) siRNA group (Fig. 2A). When the fluorescence intensity for the NC siRNA was set at 100%, the fluorescence intensity was 59.0% for EGFR siRNA, 88.8% for αvβ3 siRNA, and 77.6% for NRP-1 siRNA. It can be seen from the first panel (NC siRNA) that the strong green fluorescence of anti-EGFR-iRGD was located in the cytoplasmic region with a diffused pattern, indicating that a large number of the proteins were internalized in the cells (Fig. 2C). These results indicate that the recombinant protein anti-EGFR-iRGD possesses specificity and affinity to EGFR, αvβ3, NRP-1 and could internalize into cells.

Furthermore, the specificity and affinity of anti-EGFR-iRGD binding to the target antigen were assessed using a competitive binding assay. When fluorescence intensity for anti-EGFR-iRGD-FITC taken up by BGC-823 was set as 100%, the affinity of anti-EGFR-iRGD was decreased to 85.7% or 85.2% when 25 μg/mL of cetuximab or 10 μg/mL of iRGD final concentration was added to compete with the antigen (Fig. 2D). The binding of anti-EGFR-iRGD to BGC-823 cells was specifically inhibited by both cetuximab and iRGD, indicating that anti-EGFR-iRGD binds to the same receptor. These results indicate that anti-EGFR-iRGD possesses specificity and affinity to EGFR and is internalized through the same route as iRGD.

3.3. In vitro cytotoxicity, mechanism of recombinant proteins

To verify the pharmacological activity of anti-EGFR and anti-EGFR-iRGD, in vitro cytotoxicity tests using MTT assays against BGC-823, Caco-2 and MCF-7 (EGFR lowly expressed) [38] were conducted. It

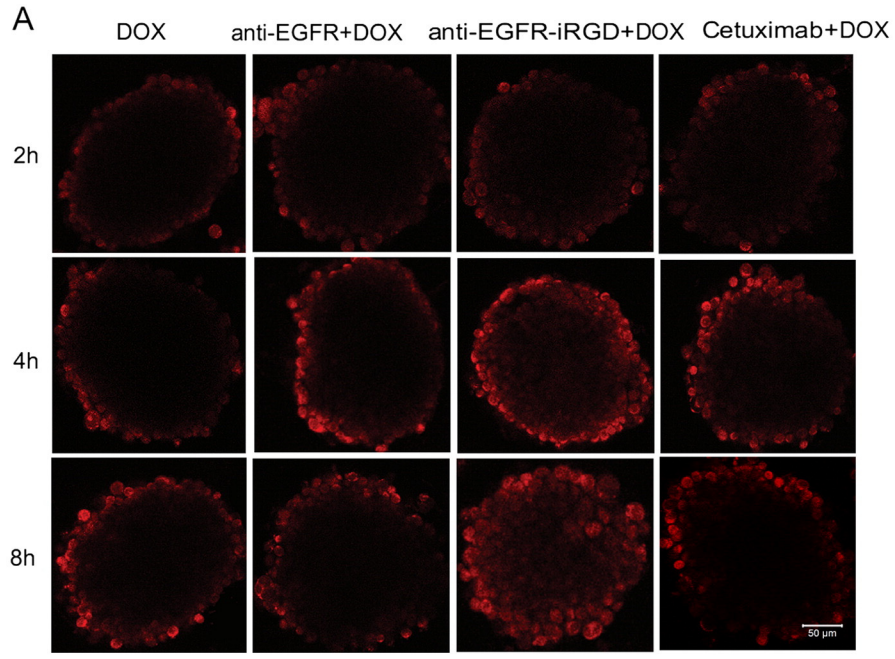
A
DOX
anti-EGFR+DOX
anti-EGFR-iRGD+DOX
Cetuximab+DOX
2h
4h
8h
50 μm

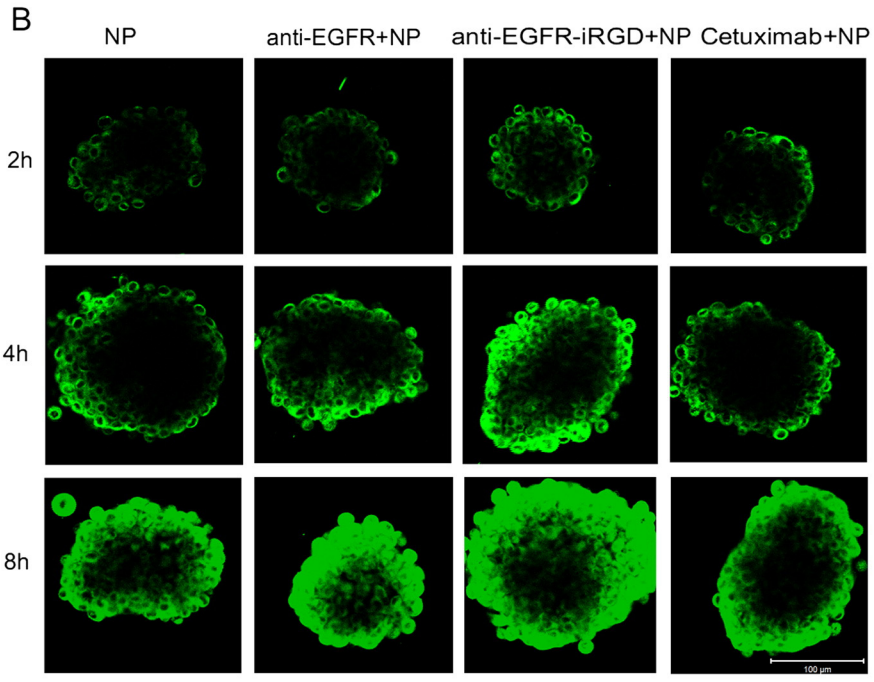
B
NP
anti-EGFR+NP
anti-EGFR-iRGD+NP
Cetuximab+NP
2h
4h
8h
100 μm

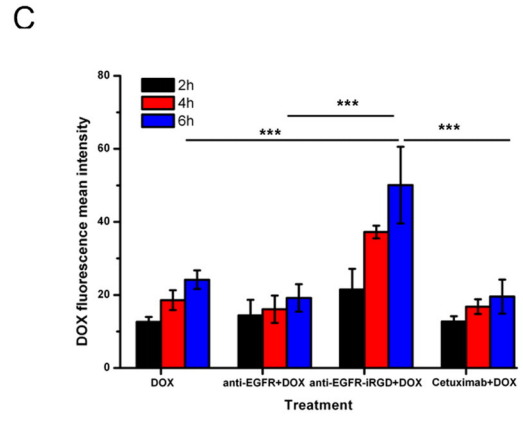
C
DOX fluorescence mean intensity
2h
4h
6h
***
***
***
DOX
anti-EGFR+DOX
anti-EGFR-iRGD+DOX
Cetuximab+DOX
Treatment

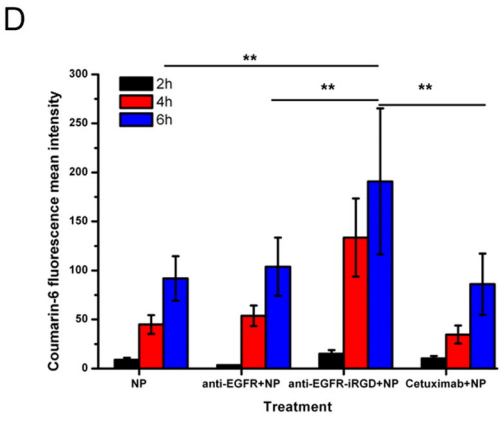
D
Coumarin-6 fluorescence mean intensity
2h
4h
6h
**
**
**
NP
anti-EGFR+NP
anti-EGFR-iRGD+NP
Cetuximab+NP
Treatment

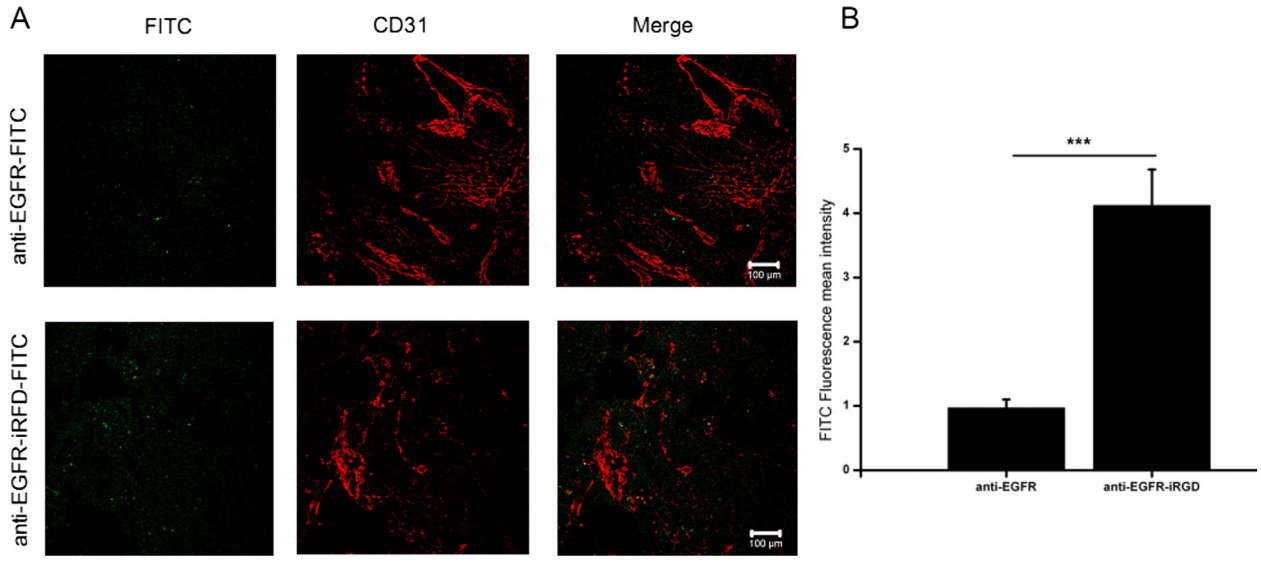

Fig. 7. Evaluation of the penetration of anti-EGFR (top) and anti-EGFR-iRGD (bottom) in BGC-823 tumors at 1 h post-injection. A, FITC labeled proteins (green) and CD31 of blood vessels (red) are shown in the images of tumor sections. Scale bar = 100 μm. B, the quantification of fluorescence intensity. (For interpretation of the references to color in this figure legend, the reader is referred to the web version of this article.)

was found that both anti-EGFR and cetuximab exhibited no anti-proliferative activity against BGC-823 cells even at the highest concentration of 240 μg/mL (Fig. 3A). However, a dose-dependent cytotoxicity was observed for anti-EGFR-iRGD. This finding indicates that the addition of the iRGD motif can improve the anti-proliferative activity of anti-EGFR in the human gastric cancer cell line BGC-823. For the Caco-2 cell line (Fig. 3B), anti-EGFR and anti-EGFR-iRGD showed notable anti-proliferative activity compared with cetuximab. Although the difference between anti-EGFR and anti-EGFR-iRGD was not significant, anti-EGFR-iRGD exhibited a slightly stronger inhibition in proliferation of Caco-2 ($p = 0.076$). For the MCF-7 cell line (low EGFR expression), no anti-proliferative activity was observed even at the highest concentration of 240 μg/mL (Fig. 3C).

To evaluate the mechanism of recombinant proteins inhibiting cancer cell proliferation, indicated concentrations of anti-EGFR, anti-EGFR-iRGD or cetuximab were added to BGC-823 cells. The cells were harvested 20 h later and the protein expression level for EGFR and active p-EGFR (Tyr1172) were analyzed using a Western blot. It was found that the phosphorylation of EGFR can be inhibited by all of the 50 μg/ml protein treatments indicating that anti-EGFR and anti-EGFR-iRGD may act like cetuximab in inhibiting EGFR Tyr1172 phosphorylation, thus inhibiting cancer cell proliferation (Supplementary Fig. S3D).

3.4. MCS growth inhibition and penetration in MCS for protein alone

BGC-823 was also used to culture the 3D tissue model called MCS. It was observed that the MCS had a symmetrical and spherical shape of about 200 μm in diameter after 7 days in culture (Fig. 4A). To study the inhibition of different treatments to MCS, BGC-823 MCS were exposed to culture medium and the recombinant protein groups (120 μg/mL) for 24 h and then incubated with fresh culture medium (changed every day) for another 6 days. The representative images of MCS that underwent different treatments indicate that MCS in the fresh culture medium and protein groups all grew during the 7 day period (Fig. 4B). It was found that the cells of MCS became very compact due to the interaction among cells and the secretion of ECM.

The alteration in mean diameter of all 4 groups can be seen in Fig. 3D. It indicates that the culture medium control group and anti-EGFR group, increased in diameter from 217 to 295 μm and 202 to 261 μm, respectively. The diameter of both anti-EGFR-iRGD and cetuximab increased more slowly over time leading to a mean diameter of 232 μm and 240 μm, respectively. It is notable that the difference in mean diameter on day 7 between both anti-EGFR-iRGD and cetuximab with the control is significant ($p < 0.05$).

The penetration ability of recombinant protein anti-EGFR and anti-EGFR-iRGD was also analyzed with MCS. At 6 h, the fluorescence signal of anti-EGFR was only localized in the vicinity of the periphery of MCS, while the penetration of anti-EGFR-iRGD was deeper than that of anti-EGFR (Fig. 4C). After 24 h of incubation, the strong fluorescence of two recombinant proteins occupied the entire MCS. For anti-EGFR at 24 h, a gradually diffused and decreased fluorescence pattern from the periphery to center region of the spheroids was evident (Fig. 4C & D). On the other hand, the fluorescence pattern of anti-EGFR-iRGD grew in intensity from the periphery to center region of the MCS (Fig. 4C & D). This demonstrates that when anti-EGFR is fused with iRGD, the penetration in MCS is significantly improved.

3.5. MCS growth inhibition and penetration in MCS for protein combined with cancer drugs

In order to investigate whether combined with anti-EGFR-iRGD could enhance the efficacy of other cancer drugs, we tested chemical drugs from a 0.6 kDa molecule up to nanoparticles. To be specific, chemical drug DOX (20 μg/mL), monoclonal antibody bevacizumab (1 mg/mL) and liposomes (1.5 μg/mL) were used. The alteration of day 7 from day 1 in mean diameter of groups (proteins, DOX, bevacizumab, paclitaxel liposomes) can be seen in Fig. 5A and B (DOX); C (bevacizumab) and D (liposomes) are part of Fig. 5A. The control group (147% of original spheroid volume on 7th day) kept growing, and the inhibition of spheroid growth by protein

Fig. 6. Penetration into MCS of DOX or PEG-PCL-Coumarin-6-NP combined with recombinant protein. A and C, LSCM images (A) and mean fluorescence intensity (C) of BGC-823 MCS incubated with DOX, DOX combined with anti-EGFR, DOX combined with anti-EGFR-iRGD, DOX combined with cetuximab for 2 h, 4 h and 8 h, respectively. B and D, LSCM images (B) and mean fluorescence intensity (D) of BGC-823 MCS incubated with PEG-PCL-Coumarin-6-NP, PEG-PCL-Coumarin-6-NP combined with anti-EGFR, PEG-PCL-Coumarin-6-NP combined with anti-EGFR-iRGD, PEG-PCL-Coumarin-6-NP combined with cetuximab for 2 h, 4 h and 8 h, respectively. Data are represented as mean ± SD (n = 3). **, $p < 0.01$. ***, $p < 0.001$. Scale bar in A = 50 μm, scale bar in B = 100 μm.

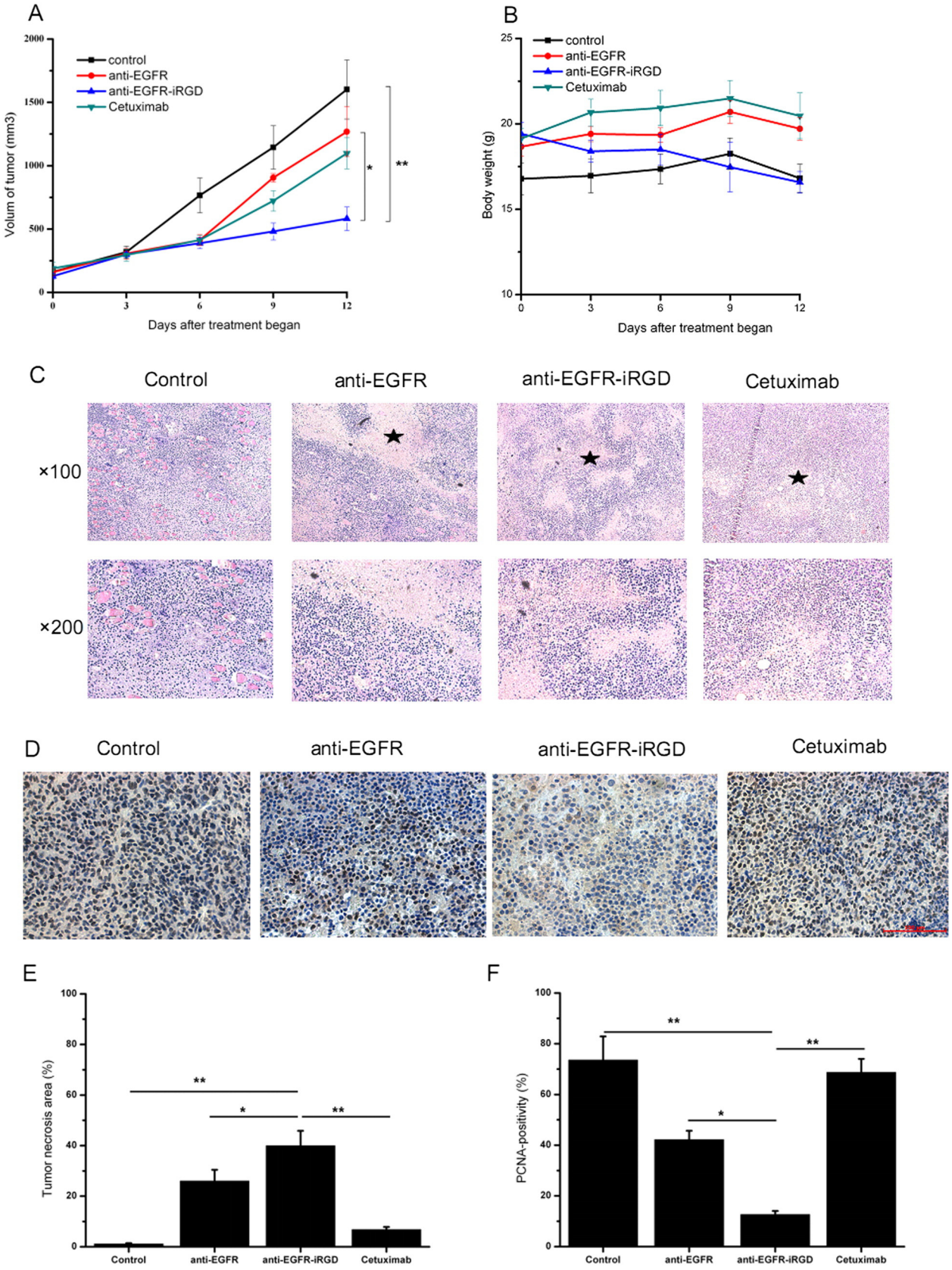

Fig. 8. Mice bearing subcutaneous BGC-823 (8 mice per treatment group) were treated by intraperitoneal injections of PBS, anti-EGFR, anti-EGFR-iRGD or cetuximab every three days. A and B, show the tumor growth curves (A) and body weight change (B) of BGC-823 tumor-bearing mice that received the indicated treatments. Data are represented as mean ± SEM (standard error of the mean) (n = 8). One-way ANOVA was used for the analysis of tumor volume and body weight. *, $p < 0.05$, **, $p < 0.01$. C and D, show analysis for cell necrosis and anti-proliferative effect of anti-EGFR and anti-EGFR-iRGD in BGC-823 tumors. Cell necrosis was evaluated by H&E staining (×100 upper, ×200 lower) of tumor sections and cell proliferation was evaluated by immunohistochemistry of PCNA (D). *, indicate the necrotic regions. Scale bar = 100 μm. E and F, the quantification of tumor necrosis area (E) and PCNA immunohistochemical positivity (F).

anti-EGFR (100 μg/mL), anti-EGFR-iRGD (100 μg/mL) and cetuximab (100 μg/mL) displayed a similar trend to the results of Fig. 3D. The treatments of DOX alone and combination groups inhibited growth of spheroids to a certain extent, the mean diameters from day 1 to day 7 were 203–206 μm for DOX, 204–196 μm for DOX combination with anti-EGFR, 200–142 μm for DOX combination with anti-EGFR-iRGD, and 199–174 μm for DOX combination with cetuximab (Fig. 5B). These results indicate that combination of anti-EGFR-iRGD with DOX can more efficiently inhibit the growth of BGC-823 MCS ($p < 0.01$).

The inhibition of spheroid growth by bevacizumab groups exhibited a similar trend to the result of DOX. It indicates that the bevacizumab group, bevacizumab + anti-EGFR, bevacizumab + anti-EGFR-iRGD and bevacizumab + cetuximab increased in diameter from 208 to 267 μm and 201 to 210 μm, and from 204 to 212 μm and 201 to 222 μm, respectively. It is notable that the difference in mean diameter on day 7 between both bevacizumab + anti-EGFR-iRGD and bevacizumab + anti-EGFR with bevacizumab was significant ($p < 0.01$). For paclitaxel liposomes of size of about 400 nm, no significant difference is observed from these four groups, which means no protein could enhance the anti-cancer property of liposomes.

Here, we also tested whether the conjugation of iRGD to the C-terminus of anti-EGFR could enhance the penetration of DOX and nanoparticles into MCS by LSCM. From Fig. 6A, the penetration of DOX in the BGC-823 MCS at 2 h was limited to the outer few cell layers of the spheroids. The fluorescence signal of DOX combination with anti-EGFR or cetuximab group was similar to DOX alone. At 4 h, the weak fluorescence signal of DOX delivered together with anti-EGCR-iRGD started appearing at the center of the MCS with strong fluorescence appeared in few outer cell layers. This indicates that some DOX could penetrate through the spheroids compared to DOX alone. After 8 h of co-incubation, a strong DOX fluorescence signal was observed spreading the whole MCS. A semi-quantitative analysis of mean fluorescence intensity of DOX in MCS indicated that anti-EGFR-iRGD could penetrate in BGC-823 MCS, and enhance DOX penetration into deeper zone of MCS ($p < 0.001$) (Fig. 6C). This is consistent with the result we observed in the growth inhibition in multicellular spheroids described above.

Coumarin-6 loaded PEG-PCL nanoparticles were prepared, and intracellular incorporation and release of coumarin-6 in BGC-823 MCS was measured by LSCM (Fig. 6B). At 2 h, the penetration of nanoparticles in the MCS was also limited to the outer few cell layers of the spheroids, which showed barely detectable levels of intracellular fluorescence. After 4 h of incubation, MCS incubated with anti-EGFR-iRGD + PEG-PCL-Coumarin-6-NP were more intensely fluorescent and showed deeper penetration of fluorescence than other groups. At 6 h, the differences of fluorescence intensity between anti-EGFR-iRGD + PEG-PCL-coumarin-6-NP and other groups were significant (Fig. 6D). We conclude that anti-EGFR-iRGD can enhance PEG-PCL nanoparticle penetration into MCS.

3.6. Penetration in tumor tissue

Next, we analyzed the penetration ability of the anti-EGFR-iRGD by using both BGC-823 bearing mice (Fig. 7) and H22 bearing ICR mice tumor tissue (Supplementary Fig. S4). Green fluorescence signal on LSCM images indicates recombinant protein's position as anti-EGFR and anti-EGFR-iRGD were labeled with FITC. In order to visualize the location of blood vessels, Alex-594-conjugated secondary antibody was complexed with primary anti-CD31 antibody. Thus, the blood vessels would exhibit red fluorescence. After 1 h post-injection, anti-EGFR was observed and localized in the vicinity of blood vessels. This result indicates that anti-EGFR sdAbs can target the tumor and extravasate through the vessels. In contrast, anti-EGFR-iRGD penetrated much farther from the tumor vessels and even localized on a much larger area in the tumor tissue compared to anti-EGFR, and the FITC fluorescence mean intensity of anti-EGFR-iRGD was four times stronger than that of anti-EGFR (Fig. 7B). H22 tumor tissues showed similar results to BGC-823 tumor tissue data. These data support the notion that iRGD as a functional group mediates active tumor penetration of the anti-EGFR protein. The result is consistent with the results of protein penetration in BGC-823 MCS (Fig. 4C & D).

3.7. Inhibitory effect of anti-EGFR-iRGD on tumor growth in mice and side effects study

We next sought to determine whether anti-EGFR-iRGD could be used as a therapeutic agent in the mice bearing subcutaneously inoculated BGC-823 tumors. Fig. 8A shows the growth curves of the BGC-823 tumors in the mice after the treatment has begun. The BGC-823 tumors grew rather rapidly in mice treated with intraperitoneal injections of PBS or anti-EGFR. By day 12, the average tumor volumes of PBS and anti-EGFR had increased about 10 fold and 8 fold, respectively. In the cetuximab treated mice the tumor volume increased about 6 fold by day 12 and the tumor volume was reduced by about 31.5% compared to the PBS control group. Significantly, in the anti-EGFR-iRGD treated mice, the tumor volume increased 4.5 fold by day 12 and the tumor volume was reduced by about 63.7% compared with the PBS control group. The differences in tumor volumes between the groups treated by anti-EGFR-iRGD and either PBS ($p < 0.01$) or anti-EGFR ($p < 0.05$) were both statistically significant.

None of the mice treated by intraperitoneal injection with PBS, anti-EGFR or cetuximab alone showed any body weight loss (Fig. 8B). Although the mean body weight of the anti-EGFR-iRGD group showed a slight decrease during the treatment, the differences in body weight between the groups treated by anti-EGFR-iRGD and other groups were not significant ($p > 0.05$).

The pathology examination clearly demonstrated tumor necrosis present in the different treatments (Fig. 8C & E). In the control group treated with PBS, there were few necrotic regions. The anti-EGFR and cetuximab treated groups showed much larger necrotic regions, and the anti-EGFR-iRGD group was observed with the largest area of necrotic regions which explains the smallest tumor volumes of the group at the pathological level. In agreement with the H&E staining, there were many tumor cells stained positively with PCNA (cells with brown nuclei) in the control group, indicating a high proliferation ability (Fig. 8D & F). The anti-EGFR and cetuximab treated groups exhibited fewer positive cells compared to the control group. Tumors from the anti-EGFR-iRGD group showed the lowest number of positive cells. No abnormal damage was observed in the H&E stained sections of the main organs (Supplementary Fig. S5).

4. Discussion

In this study, we introduced a cell-penetrating peptide (CPP), iRGD, to an EGFR sdAb and evaluated the penetration and anti-proliferation activity on gastric cancer. CPPs allow cargoes such as small molecular drugs or nanoparticles to be internalized through the cell membrane [39]. HIV-Tat [40,41] is a traditional cell-penetrating peptide without cell selectivity, and most CPPs are nonspecific. The specificity of CPP can be supplemented by combination with tumor-targeting peptides. Other kinds of CPPs have an inherent tumor targeting capacity, such as peptides with RGD (arginine/glycine/aspartic acid) or NGR (asparagine/glycine/arginine) sequences. Peptides such as iRGD, iNGR (CRNGRGPDC, iNGR) [42] or LyP-1 (CGNKRTRGC) [43] have both tumor-targeting and cell penetrating abilities. iRGD binds to the tumor marker integrin αvβ3 directly, while iNGR binds to CD13 of the tumor vessels [42], and LyP-1 binds to a mitochondrial protein p32/gC1qR/HABP1 [44] expressed at the cell surface of tumors. The peptide iRGD homed tumor cells or tumor vessels, and penetrated into the tumor cell or the tumor mass. Due to this activity, we introduced iRGD to the anti-EGFR sdAb in order to enhance the antitumor activity of the drug.

In the current study, the anti-EGFR sdAb and anti-EGFR-iRGD were both expressed successfully in *E. coli* BL21 (DE3) and purified by

nickel–nitrilotriacetic acid affinity chromatography. Our results placed anti-EGFR in the N-terminal domain and iRGD in the C-end with a linker of Gly4Ser in between. This is the first demonstration of a recombinant protein constructed by introducing sdAb to iRGD. Surface plasmon resonance analysis, an antigen–antibody binding assay and a competitive binding assay revealed that anti-EGFR-iRGD has two target antigens — EGFR and αvβ3. Most antibodies have only a single target, however, bispecific antibodies (BsAbs) with specificity for two target antigens are preferred [45]. One type of BsAb can build a bridge between an immune cell and cancer cell facilitating cell death. Another kind of BsAb can bind to two growth factor receptors expressed on tumor cells and has the advantage of generating synergistic activities [46]. EGFR and integrin (αvβ3) are receptors expressed in many tumors [8,18]. Dual targeting of EGFR and αvβ3 has a wider scope of application for amplifying tumor targeting than either mechanism alone.

Instead of two-dimensional monolayer cells (2D), multicellular spheroids (3D) culture and in vivo studies were used to investigate the cell cytotoxicity and penetration of the recombinant proteins. These results revealed that both anti-EGFR and anti-EGFR-iRGD had anti-proliferation activity, especially on the cells that highly express EGFR, and that the latter showed stronger antitumor activity. Anti-EGFR-iRGD could penetrate into deeper zone of the MCS and tumor mass. The molecular mechanism of the rapid tumor tissue penetration of iRGD remains to be elucidated. However, several lines of evidence suggest that it may involve the so-called vascular permeabilization in the tumor induced by the CendR property of iRGD. Molecules such as VEGF-165 and some semaphorins that have exposed CendR motifs increase vascular permeability [47,48]. This novel agent shows great superiority in treating gastric tumor-bearing mice, and no significant abnormal damage was observed. What is more, anti-EGFR-iRGD also promoted DOX, PEG-PCL nanoparticles penetration into MCS and enhanced the efficacy of cancer drugs DOX, bevacizumab. For PEG-PCL-Coumarin-6-NP, NP + anti-EGFR-iRGD showed strongest fluorescence intensity of all groups (Fig. 6B & D). However, there was no significant difference of diameter of MCS between paclitaxel liposome combination with anti-EGFR-iRGD and other combination groups. The reason of this phenomenon is probably the size of the nanoparticles. The mean size of PEG-PCL-NP is around 100 nm [35], but the mean size of paclitaxel liposome is much bigger (~400 nm). Thus, anti-EGFR-iRGD could not efficiently deliver paclitaxel liposome into deep zone of MCS.

Chen et al. [49] defined and constructed a recombinant protein iRGD-CDD, they confirmed iRGD-CDD spread extensively within the tumor and demonstrated CendR peptide iRGD could be active in protein transduction. Similarly, the fusion protein anti-EGFR-iRGD in our work is a promising antitumor agent capable of spreading within both MCS and tumor tissue after intravenous injection. When using MCS, the results regarding protein penetration demonstrated the improved penetration of anti-EGFR in MCS when fused with iRGD. MCS are models that reflect many of the properties of natural solid tumors. Integrin expression, such as αvβ3, in MCS is more similar to nude mice xenotransplant expression than the high expression levels found in monolayers [50]. Integrin expression has been found to be limited in the proliferating periphery cell layers or quiescent intermediate zone [25]. Thus MCS are an ideal model for studying this targeting integrin protein, anti-EGFR-iRGD. Since there is no vasculature system in BGC-823 MCS, the iRGD-induced penetration should result from neuropilin-1 (NPR-1) expressed on BGC-823 cell membrane. As Sugahara et al. mentioned, when the iRGD binds to NRP-1, a cell internalization and trans-tissue transport pathway is activated [19].

The therapeutic efficacy of anti-cancer drugs can be limited by poor penetration into tumors due to the complicated tumor microenvironment. It was found that chemical conjugation with iRGD is not required to enhance the therapeutic effects of anticancer drugs. Systemic injection with free iRGD into the mouse tumor models can enhance tumor-specific delivery and improve the therapeutic index of 10 different anti-cancer drugs including DOX, trastuzumab and nanoparticles (from a 0.6 kDa molecule up to a 130 nm particle) [37]. In the present work, the iRGD domain was set in the C-terminal and conjugated with a relatively large sdAb. The molecular weight of anti-EGFR is 16.17 kDa, while iRGD contains only 9 amino acids. Due to the linker $(Gly4Ser)_3$, the 3D structure of anti-EGFR-iRGD, investigated by molecular modeling, shows that the iRGD motif does not influence the structure of the sdAb. In addition, anti-EGFR does not impact the function of iRGD including the affinity of cyclic-RGD for integrin αvβ3 and its vascular and tissue permeability. We propose that anti-EGFR-iRGD can help improve the performance of cancer drugs, and we are currently continuing the research on the in vivo efficacy of anti-EGFR-iRGD helping both anti-cancer drugs and tumor imaging agents. This is the first time comparing the delivery efficiency of this combination regimen to that of the iRGD fusion protein.

5. Conclusion

In summary, this study represents an example of constructing a fusion protein of peptide iRGD and sdAb. We expressed and investigated the therapeutic efficacy of anti-EGFR-iRGD on monolayer cells (2D), multicellular spheroids (3D) and tumor-bearing mice for the first time. This novel agent shows great superiority in treating solid tumors, especially for gastric cancer, and could be a useful adjunct of other anticancer drugs. We are currently continuing the research of the co-administration of anti-EGFR-iRGD and other anticancer drugs or tumor imaging agents for gastric cancer and other solid tumors. There are still issues to be addressed, e.g., stability and pharmacokinetic properties of the recombinant proteins, and the mechanisms underlying the antitumor efficacy of anti-EGFR-iRGD which will be further studied to guarantee improved clinical application.

Supplementary data to this article can be found online at http://dx.doi.org/10.1016/j.jconrel.2014.12.039.

Acknowledgments

This work was supported by the National Natural Science Foundation of China(No. 81220108023, 81472216, 81302053), NIH grant CA149363, CA151652 and CA149387, Top Six Talents Project of Jiangsu Province (Grant No. WSN-007), Nanjing Medical Science and Technology Development Projects (Grant No. NJGL-2011225), the Science Fund of Jiangsu Province for Distinguished Young Scholars (BK20140049) and the Scientific Research Foundation of Graduate School of Nanjing University (2013CL15). We thank Dr. Zhiguo Chen and Dr. Chen Xie for their scientific contribution to this work.

References

[1] A. Jemal, F. Bray, M.M. Center, J. Ferlay, E. Ward, D. Forman, Global cancer statistics, CA Cancer J. Clin. 61 (2011) 69–90.
[2] R. Siegel, J. Ma, Z. Zou, A. Jemal, Cancer statistics, 2014, CA Cancer J. Clin. 64 (2014) 9–29.
[3] J.L. Teillaud, From whole monoclonal antibodies to single domain antibodies: think small, Methods Mol. Biol. 911 (2012) 3–13.
[4] M.M. Harmsen, H.J. De Haard, Properties, production, and applications of camelid single-domain antibody fragments, Appl. Microbiol. Biotechnol. 77 (2007) 13–22.
[5] M. Arbabi Ghahroudi, A. Desmyter, L. Wyns, R. Hamers, S. Muyldermans, Selection and identification of single domain antibody fragments from camel heavy-chain antibodies, FEBS Lett. 414 (1997) 521–526.
[6] S. Muyldermans, Nanobodies: natural single-domain antibodies, Annu. Rev. Biochem. 82 (2013) 775–797.
[7] S. Muyldermans, T. Atarhouch, J. Saldanha, J.A. Barbosa, R. Hamers, Sequence and structure of VH domain from naturally occurring camel heavy chain immunoglobulins lacking light chains, Protein Eng. 7 (1994) 1129–1135.
[8] D.S. Salomon, R. Brandt, F. Ciardiello, N. Normanno, Epidermal growth factor-related peptides and their receptors in human malignancies, Crit. Rev. Oncol. Hematol. 19 (1995) 183–232.
[9] M.A. Kim, H.S. Lee, H.E. Lee, Y.K. Jeon, H.K. Yang, W.H. Kim, EGFR in gastric carcinomas: prognostic significance of protein overexpression and high gene copy number, Histopathology 52 (2008) 738–746.
[10] C. Yewale, D. Baradia, I. Vhora, S. Patil, A. Misra, Epidermal growth factor receptor targeting in cancer: a review of trends and strategies, Biomaterials 34 (2013) 8690–8707.

[11] R.K. Jain, The Eugene M. Landis Award Lecture 1996. Delivery of molecular and cellular medicine to solid tumors, Microcirculation 4 (1997) 1–23.
[12] M.F. Milosevic, A.W. Fyles, R. Wong, M. Pintilie, M.C. Kavanagh, W. Levin, L.A. Manchul, T.J. Keane, R.P. Hill, Interstitial fluid pressure in cervical carcinoma: within tumor heterogeneity, and relation to oxygen tension, Cancer 82 (1998) 2418–2426.
[13] C.H. Heldin, K. Rubin, K. Pietras, A. Ostman, High interstitial fluid pressure — an obstacle in cancer therapy, Nat. Rev. Cancer 4 (2004) 806–813.
[14] R. Li, L. Xie, Z. Zhu, Q. Liu, Y. Hu, X. Jiang, L. Yu, X. Qian, W. Guo, Y. Ding, B. Liu, Reversion of pH-induced physiological drug resistance: a novel function of copolymeric nanoparticles, PLoS One 6 (2011) e24172.
[15] P.A. Netti, D.A. Berk, M.A. Swartz, A.J. Grodzinsky, R.K. Jain, Role of extracellular matrix assembly in interstitial transport in solid tumors, Cancer Res. 60 (2000) 2497–2503.
[16] L. Davies Cde, D.A. Berk, A. Pluen, R.K. Jain, Comparison of IgG diffusion and extracellular matrix composition in rhabdomyosarcomas grown in mice versus in vitro as spheroids reveals the role of host stromal cells, Br. J. Cancer 86 (2002) 1639–1644.
[17] E. Brown, T. McKee, E. diTomaso, A. Pluen, B. Seed, Y. Boucher, R.K. Jain, Dynamic imaging of collagen and its modulation in tumors in vivo using second-harmonic generation, Nat. Med. 9 (2003) 796–800.
[18] U.K. Marelli, F. Rechenmacher, T.R. Sobahi, C. Mas-Moruno, H. Kessler, Tumor targeting via integrin ligands, Front. Oncol. 3 (2013) 222.
[19] K.N. Sugahara, T. Teesalu, P.P. Karmali, V.R. Kotamraju, L. Agemy, O.M. Girard, D. Hanahan, R.F. Mattrey, E. Ruoslahti, Tissue-penetrating delivery of compounds and nanoparticles into tumors, Cancer Cell 16 (2009) 510–520.
[20] T. Teesalu, K.N. Sugahara, V.R. Kotamraju, E. Ruoslahti, C-end rule peptides mediate neuropilin-1-dependent cell, vascular, and tissue penetration, Proc. Natl. Acad. Sci. U. S. A. 106 (2009) 16157–16162.
[21] W.R. Inch, J.A. McCredie, R.M. Sutherland, Growth of nodular carcinomas in rodents compared with multi-cell spheroids in tissue culture, Growth 34 (1970) 271–282.
[22] R.M. Sutherland, J.A. McCredie, W.R. Inch, Growth of multicell spheroids in tissue culture as a model of nodular carcinomas, J. Natl. Cancer Inst. 46 (1971) 113–120.
[23] T. Nederman, B. Norling, B. Glimelius, J. Carlsson, U. Brunk, Demonstration of an extracellular matrix in multicellular tumor spheroids, Cancer Res. 44 (1984) 3090–3097.
[24] R.M. Sutherland, Cell and environment interactions in tumor microregions: the multicell spheroid model, Science 240 (1988) 177–184.
[25] G. Hamilton, Multicellular spheroids as an in vitro tumor model, Cancer Lett. 131 (1998) 29–34.
[26] A. Ivascu, M. Kubbies, Rapid generation of single-tumor spheroids for high-throughput cell function and toxicity analysis, J. Biomol. Screen. 11 (2006) 922–932.
[27] A.I. Minchinton, I.F. Tannock, Drug penetration in solid tumours, Nat. Rev. Cancer 6 (2006) 583–592.
[28] T.W. Hambley, W.N. Hait, Is anticancer drug development heading in the right direction? Cancer Res. 69 (2009) 1259–1262.
[29] T. Murase, L. Eugenio, M. Schorr, G. Hussack, J. Tanha, E.N. Kitova, J.S. Klassen, K.K. Ng, Structural basis for antibody recognition in the receptor-binding domains of toxins A and B from *Clostridium difficile*, J. Biol. Chem. 289 (2014) 2331–2343.
[30] J. Chen, H. Chen, Y. Shi, F. Hu, X. Lao, X. Gao, H. Zheng, W. Yao, Probing the effect of the non-active-site mutation Y229W in New Delhi metallo-beta-lactamase-1 by site-directed mutagenesis, kinetic studies, and molecular dynamics simulations, PLoS One 8 (2013) e82080.
[31] A. Bell, Z.J. Wang, M. Arbabi-Ghahroudi, T.A. Chang, Y. Durocher, U. Trojahn, J. Baardsnes, M.L. Jaramillo, S. Li, T.N. Baral, M. O'Connor-McCourt, R. Mackenzie, J. Zhang, Differential tumor-targeting abilities of three single-domain antibody formats, Cancer Lett. 289 (2010) 81–90.
[32] G.Y. Lee, P.A. Kenny, E.H. Lee, M.J. Bissell, Three-dimensional culture models of normal and malignant breast epithelial cells, Nat. Methods 4 (2007) 359–365.
[33] T.H. Kim, C.W. Mount, W.R. Gombotz, S.H. Pun, The delivery of doxorubicin to 3-D multicellular spheroids and tumors in a murine xenograft model using tumor-penetrating triblock polymeric micelles, Biomaterials 31 (2010) 7386–7397.
[34] X. Wang, X. Zhen, J. Wang, J. Zhang, W. Wu, X. Jiang, Doxorubicin delivery to 3D multicellular spheroids and tumors based on boronic acid-rich chitosan nanoparticles, Biomaterials 34 (2013) 4667–4679.
[35] Q. Liu, R.T. Li, H.Q. Qian, J. Wei, L. Xie, J. Shen, M. Yang, X.P. Qian, L.X. Yu, X.Q. Jiang, B.R. Liu, Targeted delivery of miR-200c/DOC to inhibit cancer stem cells and cancer cells by the gelatinases-stimuli nanoparticles, Biomaterials 34 (2013) 7191–7203.
[36] Z. Zhu, C. Xie, Q. Liu, X. Zhen, X. Zheng, W. Wu, R. Li, Y. Ding, X. Jiang, B. Liu, The effect of hydrophilic chain length and iRGD on drug delivery from poly(epsilon-caprolactone)-poly(N-vinylpyrrolidone) nanoparticles, Biomaterials 32 (2011) 9525–9535.
[37] K.N. Sugahara, T. Teesalu, P.P. Karmali, V.R. Kotamraju, L. Agemy, D.R. Greenwald, E. Ruoslahti, Coadministration of a tumor-penetrating peptide enhances the efficacy of cancer drugs, Science 328 (2010) 1031–1035.
[38] Y. Watanabe, R. Asano, K. Arai, I. Shimomura, H. Ogata, H. Kawaguchi, H. Hayashi, H. Ohtsuka, H. Yoshida, Y. Katayose, S. Egawa, T. Nakanishi, M. Umetsu, H. Yasui, T. Ishida, K. Imai, T. Kudo, M. Unno, I. Kumagai, In vitro and in vivo antitumor effects of recombinant bispecific antibodies based on humanized anti-EGFR antibody, Oncol. Rep. 26 (2011) 949–955.
[39] R.J. Boohaker, M.W. Lee, P. Vishnubhotla, J.M. Perez, A.R. Khaled, The use of therapeutic peptides to target and to kill cancer cells, Curr. Med. Chem. 19 (2012) 3794–3804.
[40] M. Green, P.M. Loewenstein, Autonomous functional domains of chemically synthesized human immunodeficiency virus tat trans-activator protein, Cell 55 (1988) 1179–1188.
[41] A.D. Frankel, C.O. Pabo, Cellular uptake of the tat protein from human immunodeficiency virus, Cell 55 (1988) 1189–1193.
[42] L. Alberici, L. Roth, K.N. Sugahara, L. Agemy, V.R. Kotamraju, T. Teesalu, C. Bordignon, C. Traversari, G.P. Rizzardi, E. Ruoslahti, De novo design of a tumor-penetrating peptide, Cancer Res. 73 (2013) 804–812.
[43] P. Laakkonen, K. Porkka, J.A. Hoffman, E. Ruoslahti, A tumor-homing peptide with a targeting specificity related to lymphatic vessels, Nat. Med. 8 (2002) 751–755.
[44] V. Fogal, L. Zhang, S. Krajewski, E. Ruoslahti, Mitochondrial/cell-surface protein p32/gC1qR as a molecular target in tumor cells and tumor stroma, Cancer Res. 68 (2008) 7210–7218.
[45] R.E. Kontermann, Dual targeting strategies with bispecific antibodies, MAbs 4 (2012) 182–197.
[46] S.M. Lewis, X. Wu, A. Pustilnik, A. Sereno, F. Huang, H.L. Rick, G. Guntas, A. Leaver-Fay, E.M. Smith, C. Ho, C. Hansen-Estruch, A.K. Chamberlain, S.M. Truhlar, E.M. Conner, S. Atwell, B. Kuhlman, S.J. Demarest, Generation of bispecific IgG antibodies by structure-based design of an orthogonal Fab interface, Nat. Biotechnol. 32 (2014) 191–198.
[47] H. Jia, A. Bagherzadeh, B. Hartzoulakis, A. Jarvis, M. Lohr, S. Shaikh, R. Aqil, L. Cheng, M. Tickner, D. Esposito, R. Harris, P.C. Driscoll, D.L. Selwood, I.C. Zachary, Characterization of a bicyclic peptide neuropilin-1 (NP-1) antagonist (EG3287) reveals importance of vascular endothelial growth factor exon 8 for NP-1 binding and role of NP-1 in KDR signaling, J. Biol. Chem. 281 (2006) 13493–13502.
[48] L.M. Acevedo, S. Barillas, S.M. Weis, J.R. Gothert, D.A. Cheresh, Semaphorin 3A suppresses VEGF-mediated angiogenesis yet acts as a vascular permeability factor, Blood 111 (2008) 2674–2680.
[49] R. Chen, G.B. Braun, X. Luo, K.N. Sugahara, T. Teesalu, E. Ruoslahti, Application of a proapoptotic peptide to intratumorally spreading cancer therapy, Cancer Res. 73 (2013) 1352–1361.
[50] S. Hauptmann, C. Denkert, H. Lohrke, L. Tietze, S. Ott, B. Klosterhalfen, C. Mittermayer, Integrin expression on colorectal tumor cells growing as monolayers, as multicellular tumor spheroids, or in nude mice, Int. J. Cancer 61 (1995) 819–825.